HUMAN PSYCHOPHYSICS FOR TELETACTION SYSTEM DESIGN

Gabriel Moy, Ujjwal Singh, Eden Tan, and Ronald S. Fearing
Department of Electrical Engineering and Computer Science
University of California
Berkeley, CA 94720-1770
{gmoy, ujjwal, edentan, ronf}@robotics.eecs.berkeley.edu

ABSTRACT

In this paper, we quantify several perceptual capabilities of the human tactile system needed for teletaction. We develop a model of a teletaction system based on predicted subsurface strain. Psychophysics experiments measure the spatial resolution of the human tactile system, the effects of shear stress on grating orientation discrimination, and the effects of viscoelasticity on tactile perception. The results are used to determine teletaction system design parameters. We find that 3.5-bits of amplitude resolution is sufficient for a teletaction system with a 2 mm elastic layer and 2 mm tactor spacing.

1 INTRODUCTION

Information about texture, local compliance, and local shape is important in applications such as telesurgery or handling of fragile objects in telerobotics. Figure 1 shows a general configuration of a teletaction system. One possible application is on a robotic laparoscopic telesurgery system. The tactile sensor is mounted on the end effector (the laparoscopic instrument), and the tactile display is mounted on the master manipulator (the user interface). The tactile display presents information recorded by the tactile sensor to the user. Ideally, the patterns felt by the user would be indistinguishable from direct contact with the environment. The tactile display needs to generate surface stresses that realistically represent data collected by the tactile sensor. To fully control surface stress, the ideal tactile display system would be an infinite density array of 3 DOF actuators.

Teletaction systems are composed of a tactile sensor, a tactile filter, and a tactile display. We discuss fingertip teletaction systems with high spatial detail but low temporal resolution. Most teletaction work has focused on tactile sensors and displays [Shimoga 1992; Howe et al 1995]. Tactile sensors are comparatively well understood [Howe 1994], but are generally designed for shape recognition and manipulation tasks, not teletaction. Typical tactile sensors range in size from a 1 mm square with 8×8 elements [Gray and Fearing 1996] to a 16 mm square with 8×8 elements [Howe et al 1995] to a 25 mm diameter cylinder with 3×16 elements [Nicolson and Fearing 1995]. Tactile sensors typically respond to the normal component of strain though there are tactile sensors that measure normal and shear stress [Domenici and DeRossi 1992].

A tactile filter converts tactile sensor data to tactile display data.

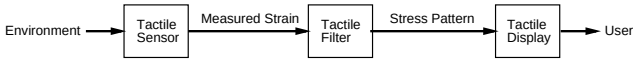

Figure 1: A block diagram representation of a general teletaction system.

Some concerns of tactile filter design include spatial and temporal sampling differences between the sensor and display, anomaly and noise filtering of the sensor data, and conversion of strain profiles from the sensor to normal and shear displacement profiles or normal and shear force profiles for the display. The filters are typically computers with A/D and D/A boards.

Tactile displays originated with tactile reading aids for the blind using piezoelectric-driven pins and direct pneumatic actuation [Bliss 1969]. Progress in tactile displays has been slow, due to the demanding mechanical requirements. An ideal display requires 50 N/cm^2 peak pressure, 4 mm stroke, and 50 Hz bandwidth; that is, a power density of 10 W/cm^2 with an actuator density of 1 per mm^2. Tactile display designs have used solenoids [Fischer et al 1995], shape memory alloy [Howe et al 1995; Hasser and Daniels 1996], pneumatics [Cohn et al 1992; Caldwell et al 1999], and MEMS [Ghodssi et al 1996]. Voice coil actuators have also been used [Pawluk et al 1998], but result in a large apparatus. Electrocutaneous stimulation [Kaczmarek et al 1991] is mechanically quite simple; however, the perceptual effects are hard to analyze. Typically, tactile displays control either displacements or forces. In a displacement display, an array of pins is shaped into a contour. In a force display, the pin array will produce a surface stress distribution representing the data. The tactile display's spatial density is limited by actuator size. Currently, the spacing between the centers of the pins is around 2 mm [Cohn et al 1992; Howe et al 1995].

Human tactile perception is not as well understood as the human vision system. Some areas, such as human tactile sensing sensitivity, sensor density, and spatial and temporal frequency response have been studied [Phillips and Johnson 1981; Loomis and Lederman 1986; Shimojo et al 1997]. We discuss teletaction displays that map information which stimulate the slowly adapting (SA I) mechanoreceptors. The SA I mechanoreceptors are at an approximate density of 70 sensors per cm^2 [Valbo and Johansson 1979]. Neurophysiological studies suggest that the SA I mechanoreceptors are most important in small-scale perception

[LaMotte and Srinivasan 1987], have a receptive field diameter of 3-4 mm, and a frequency range of 2-32 Hz [Johansson et al 1982]. Spatial resolution tests show that the 75% thresholds for gap detection and grating detection are 0.87 mm and 0.5 mm, respectively [Johnson and Phillips 1981]. Other studies show the enhanced detection of surface roughness by reducing shear stress information [Lederman 1978] and the effects of grating resolution perception due to amplitude variations [Weisenberger et al 1998]. The dynamic response of the human finger to objects with and without surface roughness is analyzed with finite element modeling [Maeno and Kobayashi 1998].

In this paper, we develop models and conduct psychophysics experiments to determine parameters for teletaction system design. In Section 2, we present a planar linear elastic model of a teletaction system, a viscoelastic model of the finger, an error model due to aliasing, and a noise model of the teletaction system. In Section 3, we describe four psychophysics experiments. Experiment 1 measures the spatial resolution of the human tactile system. Experiment 2 determines the effects of shear stress on grating orientation discrimination. Experiment 3 measures the viscoelastic parameters of the human finger pulp. Experiment 4 determines the effects of viscoelasticity on tactile perception. In Section 5, we use the results to establish the design specifications of a teletaction system.

2 MODELS

In this section, we present a planar linear elastic model for system analysis, a linear system model of a teletaction system, a simple Kelvin model for the viscoelastic properties of the human finger, and an analysis of sampling and aliasing effects. We use these models to predict the stress or strain profile applied to the mechanoreceptors during both direct contact and teletaction. With the predicted profiles, we formulate algorithms to minimize the error between direct contact and teletaction.

2.1 Planar Linear Elastic Model

A compliant tactile sensor provides contact information from objects in the environment. For simplicity, we use the plane-stress approximation (Figure 2). Consider a slice of elastic material in the $x - z$ plane with the applied force on top constant in the y direction, and the normal stresses on the face of the slice equal to 0 (σ_y = 0). (See [Fearing 1990] for explanation of assumptions).

The stresses in the slice for a line load applied normal to the surface are [Johnson, 1985]:

$$\sigma_x = \frac{-2F_z z x^2}{\pi r^4} \ , \ \ \sigma_z = \frac{-2F_z z^3}{\pi r^4} \ , \ \ \tau_{xz} = \frac{-2F_z z^2 x}{\pi r^4} \ , \qquad (1)$$

where F_z is the force per unit thickness of the slice in N/m, and $r^2 = x^2 + z^2$. For a concentrated tangential force F_x at the surface:

$$\sigma_x = \frac{-2F_x x^3}{\pi r^4} \ , \ \ \sigma_z = \frac{-2F_x x z^2}{\pi r^4} \ , \ \ \tau_{xz} = \frac{-2F_x z x^2}{\pi r^4} \ . \qquad (2)$$

Since $\sigma_y = 0$ in the plane-stress approximation, the strains ϵ_x and ϵ_z will be a function of only σ_x and σ_z:

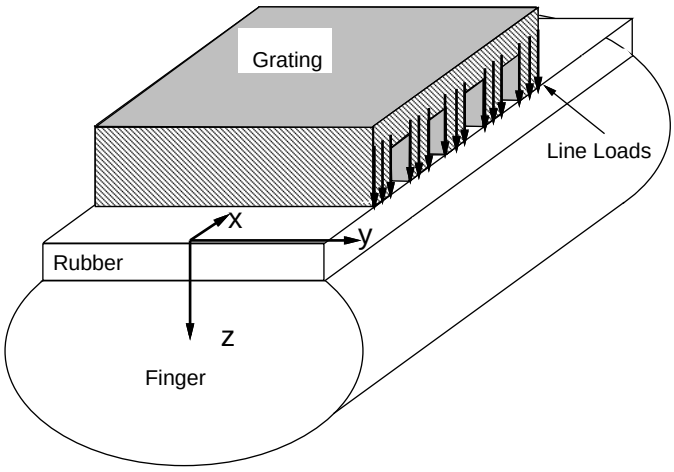

Figure 2: Finger geometry for plane stress assumption.

$$\epsilon_z \ = \ \frac{1}{E}[\sigma_z - \nu\sigma_x] \ , \ \ \epsilon_x \ = \ \frac{1}{E}[\sigma_x - \nu\sigma_z] \ , \qquad (3)$$

where E is the elastic modulus (N/m^2), and ν is Poisson's ratio (typically $\nu \approx 0.5$ for incompressible materials).

The normal strain ϵ_z has a component $h_z(x,z)$ due to the normal force component F_z and a component $h_x(x,z)$ due to the tangential force component F_x. The impulse response for normal strain (with a unit line load applied at angle α) is defined as:

$$h(x,z) \ = \ h_z(x,z)\cos\alpha \ + \ h_x(x,z)\sin\alpha \ . \qquad (4)$$

These simplified, planar models make reasonable predictions of the stress and subsurface strain profiles for various stimuli [Phillips and Johnson 1981; Shimojo 1994; Fearing 1990]. Using the linear elastic half plane assumptions, a finite element analysis predicts the subsurface strain measured by tactile sensors [Ellis and Qin 1994].

2.2 Viscoelastic Finger Model

While an elastic analysis is a good start for modeling the human finger, a viscoelastic model is a more accurate model [Fung 1993; Pawluk 1999]. The finger has viscoelastic memory which is the history of strain affecting the stress. There is considerable difference in stress response to loading and unloading. This discrepancy has lead to work in characterizing soft tissues using linear viscoelastic models. It is reasonable to assume that for oscillations of small amplitude about an equilibrium state, the theory of linear viscoelasticity should apply [Sladek and Fearing 1990].

A viscoelastic material exhibits features of hysteresis, stress relaxation, and creep. Hysteresis is defined as the difference in the stress-strain relationship during loading and unloading. Creep refers to the fact that when a body is subject to a force step, and the force is maintained, the body continues to deform. Finally, stress

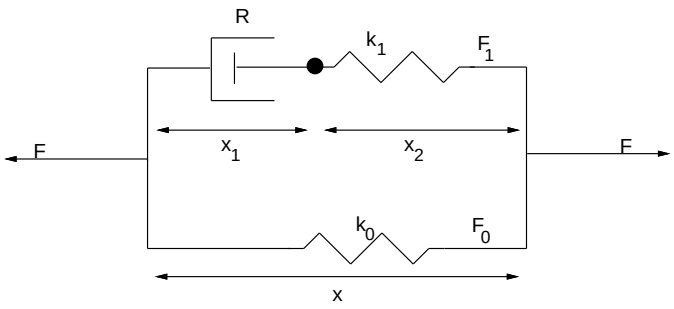

Figure 3: A Kelvin body.

relaxation refers to the property that when a position step is suddenly applied to a body, and the deformation is maintained constant afterward, the corresponding stresses in the body decrease with time.

Viscoelastic materials are often discussed in terms of mechanical models. The Kelvin model (Figure 3) is the most general relationship that includes the load, the deflection, and their first derivatives. It consists of a series connection of a dashpot (with viscosity R) and a spring (with spring constant k_1) in parallel with another spring (with spring constant k_0). In Figure 3, x refers to the displacement and F is the total force. The differential equation relating the force and the displacement is given by [Fung 1993]

$$F + \tau_\epsilon \dot{F} = E_R(x + \tau_\sigma \dot{x}) \tag{5}$$

with initial condition

$$\tau_\epsilon F(0) = E_R \tau_\sigma x(0) \tag{6}$$

where τ_ϵ (the relaxation time for constant strain), τ_σ (relaxation time for constant stress), and E_R (relaxed elastic modulus) are functions of R, k_0, k_1. Solving equation (5) with initial conditions given by equation (6) and x(t)=u(t) (the unit-step function), we obtain the relaxation function as [Fung 1993]:

$$F(t) = k(t) = E_R[1 - \frac{(\tau_\epsilon - \tau_\sigma)}{\tau_\epsilon} e^{\frac{-t}{\tau_\epsilon}}]u(t) \tag{7}$$

The form of the relaxation function is shown in Figure 4a.

Solving equation 5 with the same initial conditions and F(t)=u(t), we get the elongation produced by a sudden application of a constant force. This is called a creep function and is shown in Figure 4b and is represented by equation (8).

$$c(t) = \frac{1}{E_R}[1 - \frac{(\tau_\sigma - \tau_\epsilon)}{\tau_\sigma} e^{\frac{-t}{\tau_\sigma}}]u(t) \tag{8}$$

2.3 Teletaction System Model

A teletaction system ideally provides the operator with the sensation that his or her own finger is touching the remote surface.

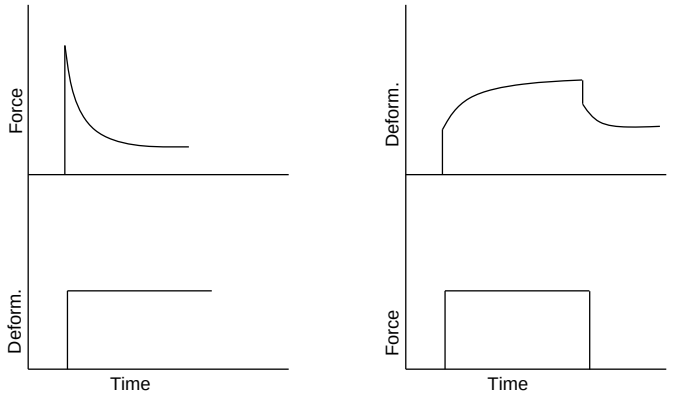

Figure 4: Relaxation and creep function for a Kelvin body.

The key problem is to find a set of forces which most closely approximates the actual contact. We define three types of teletaction systems: *Strain Matching*, *Stress Matching*, and *Shape Matching*. Consider a finger touching an object through an elastic layer which ideally has the same elastic modulus and Poisson's ratio as the idealized finger. For ideal *Strain Matching*, we need a tactile display which generates identical strain in the finger mechanoreceptors as in real contact. For ideal *Stress Matching*, we need a tactile display which generates identical stresses (to within the spatial sampling limit) on the finger surface. For ideal *Shape Matching*, we need a tactile display which can generate any arbitrary shape on the finger surface.

Tactile array displays need a spatial low pass filter to address aliasing and safety issues. Consider the spatial impulse response of the teletaction system, i.e. the response to a pin prick. If the tactile sensor does not have a spatial low-pass filter, it is impossible to localize the pin to better than one tactel no matter how tightly the sensors are packed into the array. The pin might end up between sensors and not be sensed.

Since it is very difficult to achieve a tactile display with actuator density comparable to human SA I mechanoreceptor density of approximately 70 per cm^2, an elastic layer is used as a low-pass filter so that the user feels a smooth contact instead an array of pins. If high-density high-stress actuators were available for a display, an elastic layer would then be necessary to prevent skin damage when touching sharp objects. Thus, an ideal teletaction system feels like touching the real world through an elastic layer, or glove. The higher the sensor and display density, the thinner the glove can be without introducing spatial sampling artifacts. Two simple ways to implement a spatial low-pass filter are to either attach an elastic layer over the tactile array display or attach an elastic layer over the user's finger.

Stress Matching

Consider the real contact of Figure 5 replaced with a tactile display such that the normal and shear stresses on the finger $\sigma_z(x, z = d)$, $\tau_{xz}(x, z = d)$ are the same to within the noise sensitivity of the finger (Figure 6). Ideally, the normal and shear stresses on the boundary $z = \frac{d}{2}$ are continuously sensed and ex-

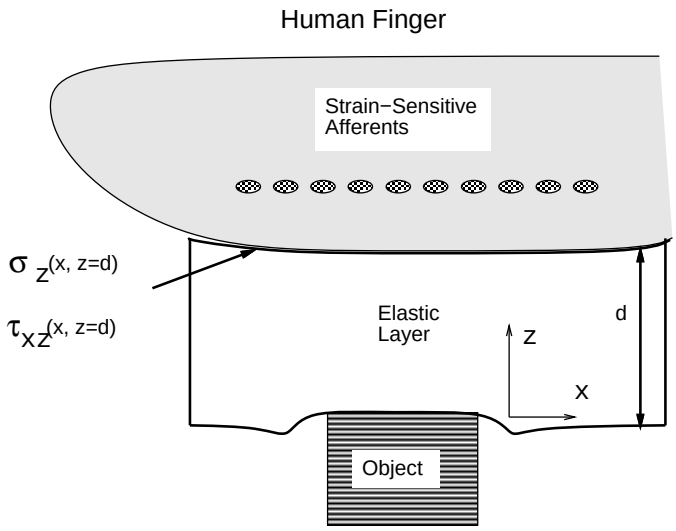

Figure 5: Example direct contact with rigid object through elastic layer.

actly replicated on the elastic layer next to the finger. Since the boundary conditions match at $z = \frac{d}{2}^+$ and at $z = \frac{d}{2}^-$, the two layers act as one layer of thickness d. Thus the finger would sense exactly what is sensed in Figure 5.

The tactile sensor measurements are spatially sampled, so information is lost due to aliasing and quantization. Since current tactile array displays can only control normal forces from each actuator, the problem is to choose the display forces, F_{ij}, so that the stress on the human finger is as close as possible to the real contact stress.

Strain Matching

Instead of matching surface stresses, we can match strains. This could be an easier problem, as the cutaneous mechanoreceptors may respond best to only one component of strain; i.e. they are scalar rather than tensor sensor elements. Johnson and Phillips [1981] suggest that an individual SA I mechanoreceptor's response correlates best with the maximum compressive strain, independent of direction. Strain energy density is another model for the mechanoreceptors [Srinivasan and Dandekar 1996, Maeno and Kobayashi 1998], which has a qualitatively better fit with the SA I mechanoreceptor data. For this paper, we use normal strain ϵ_z and assume a frictionless indentation for simplicity and the fact that robot tactile sensors typically measure normal strain. Determination of stresses and strains in a real finger would be complicated without giving more insight to the basic problem.

Using a linear, space-invariant model for the elastic medium, the normal strain at depth d for surface normal load $p(x)$ is $\epsilon_z(x, z = d) = h_z(x, d) * p(x)$. Discretizing the problem,

$$\epsilon_s = E_s p \quad (9)$$

$$\epsilon_f = E_f S f \quad (10)$$

where ϵ_f is the strain in the human finger, ϵ_s is measured strain in

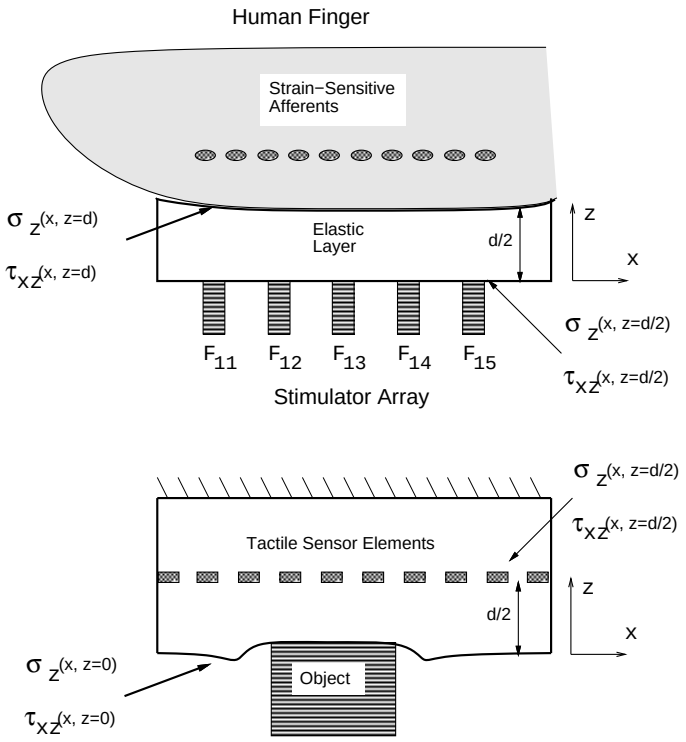

Figure 6: Tactile sensor and tactile display principles for stress matching.

the tactile sensor, E_s and E_f are the maps from surface pressure to measured strain in the sensor and finger respectively, p is the pressure on the sensor, f is the discrete set of tactile display points applying normal forces to the finger, and S is a sampling matrix. The sampling matrix inserts zero force elements to match the size of the map matrix E_f. For the ideal strain matching method, we want $\epsilon_f = \epsilon_s$.

Using a least-squares approach, the optimal force vector can be found from

$$f = [(E_f S)^T (E_f S)]^{-1} (E_f S)^T \epsilon_s . \quad (11)$$

As high sensing density is easier to achieve than high actuator density, we assume that $\epsilon_s(x)$ can be accurately recovered by interpolation. We note several difficulties with this approach, such as changes in position and temporal scales, viscoelastic effects, non-linearities, and that the human finger likely measures maximum compressive strain or strain energy density, not normal strain. Although low-pass filtering the tactile sensor makes the inverse map poorly conditioned, it also lowers required tactile display spatial resolution. Note that while f may be poorly reconstructed, it will be low-pass filtered by $E_f S$.

Let us consider a numerical example showing strain matching for a rectangular indentor (Figure 7). We assume a stimulator spacing of 1 mm, sensor depth of 1.5 mm, and rectangular indentor width of 4 mm. (For calculation, pressure and strain are discretized at 0.1 mm spacing). Figure 8 shows the good matching between normal strain in tactile sensor ϵ_s and the resulting strain

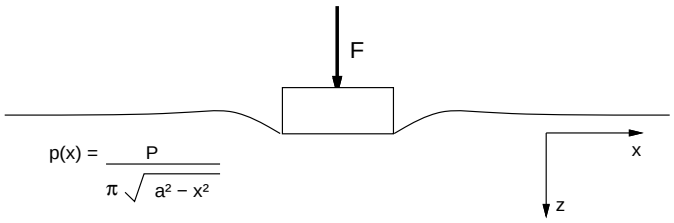

Figure 7: Example pressure distribution for rectangular indentor with frictionless indentation.

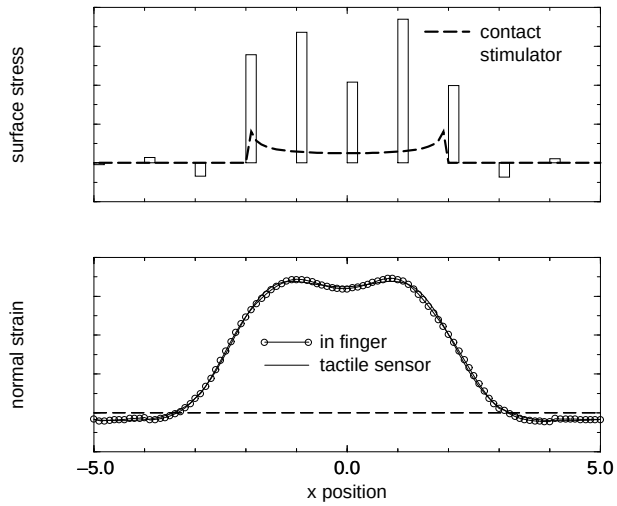

Figure 8: Equivalence of sampled surface stress profile and actual surface stress when measured by sub-surface strain sensors such as in the human finger. The top graph compares surface stress on the tactile sensor with the discrete surface stress which would be generated by a tactile display. The bottom graph compares the normal strain component in the tactile sensor and in a user's finger.

in the finger ϵ_f. Note that the stimulator values have not been regularized, hence the noisy appearance. Approaches described in [Nicolson and Fearing 1993] or [Ellis and Qin 1994] could regularize the tactor forces and ensure that they are all compressive. The elastic layer between the display pins and finger has in effect regularized the surface stress, and the sensed strain in the finger could be quite similar to the sensed strain in the tactile sensor.

Shape Matching

An alternative method for teletaction is to "... reproduce the object's contour so that it contacts the appropriate part of the human hand" [Hagner and Webster 1988]. While the concept seems appealing, it has some limitations. First, as seen in Figure 7, the surface deflection on the tactile sensor is not the same as the object shape – a shape-and-pressure from strain problem must be solved first to recover object shape and contact extent [Nicolson and Fearing, 1993]. In fact, a similar poorly conditioned map as

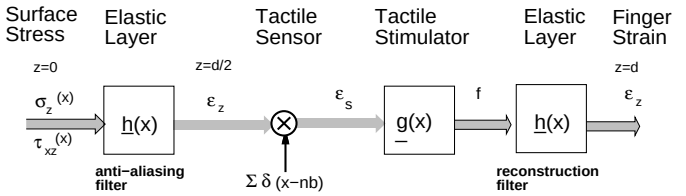

Figure 9: Signal flow model for a strain matching tactile sensor and display combination.

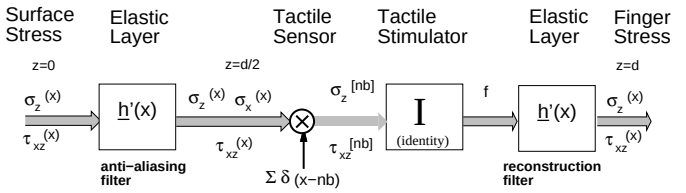

Figure 10: Signal flow model for a stress matching tactile sensor and display combination.

in equation (11) would be needed for shape display. The net loading on the finger would need to be controlled to insure that contact areas and stresses were consistent with the tactile sensor. Additionally, the shape display makes it difficult to account for shear stresses or tensile forces, which may be possible with a stress or strain matching approach.

2.4 Aliasing

Aliasing arises in the teletaction system from spatial sampling by the tactile sensor and display. In the signal flow model for *Strain Matching* (Figure 9) (or *Stress Matching* (Figure 10)), $\underline{h}(x)$ is the strain ($\underline{h'}(x)$ is the stress) response for an elastic layer of thickness $\frac{d}{2}$. The filter function $\underline{g}(x)$ converts discrete strain samples from the tactile sensor to a discrete set of forces F_{ij}, for example using equation (11). With *Stress Matching*, we directly apply measured stress samples to the finger. Typically, the normal component of strain, ϵ_z, or the normal and shear components of stress, σ_z and τ_{xz}, will be sampled, and only normal components of force will be applied by the tactile display. In signal processing terms, the elastic layers function as an anti-aliasing filter and a reconstruction filter. The amount of aliasing depends on the variable $\psi = \frac{b}{d/2}$, the ratio between sampling period, b, and the depth of a rubber layer, $\frac{d}{2}$.

Reconstruction with and without Shear Stress

In addition to aliasing, reconstruction errors also arise since current tactile displays are incapable of controlling each element's surface shear stress. Thus, it is necessary to model the system without transmission of shear stress. In some applications, such as telesurgery, the environment is slippery and is close to being frictionless, which leads to small shear forces on the surface. However, zero shear stress on the surface does not imply

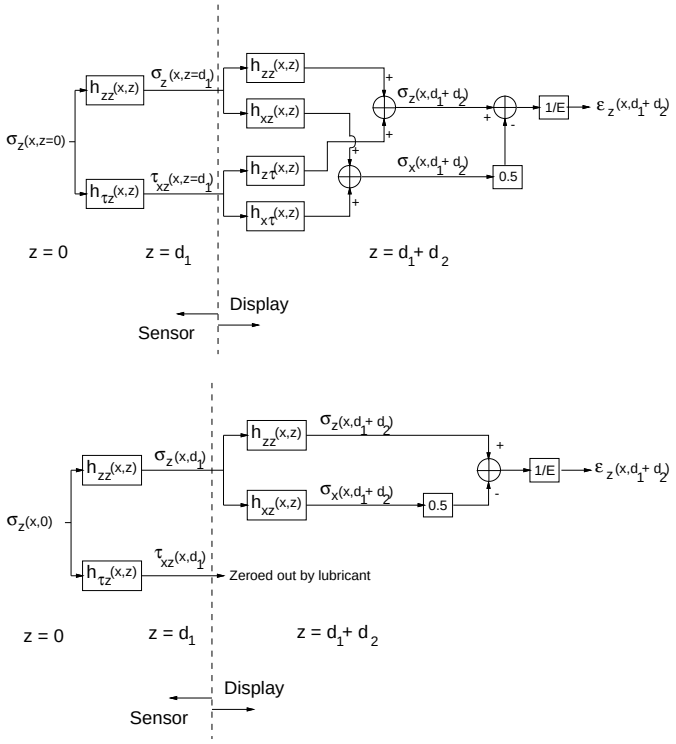

Figure 11: Block diagrams of the system reconstruction with two elastic layers a) with τ_{xz}, b) without τ_{xz} being transmitted to the display.

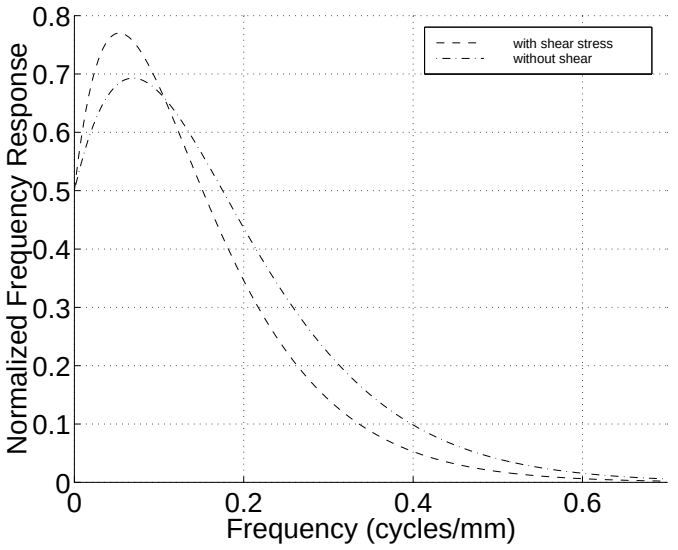

Figure 12: Normalized frequency responses of the block diagrams in Figure 11 when d = 2.7 mm (1.0 mm for each rubber layer and 0.7 mm for the SA I mechanoreceptor depth).

zero shear stress at depth $\frac{d}{2}$.

To see the effects with and without the transmission of shear stress τ_{xz} at depth $\frac{d}{2}$, a stress matching approach is used for the case of a normal line load contact. Block diagrams for the two systems are shown in Figure 11. The frequency response for the two systems are shown in Figure 12.

To calculate the normal strain in the finger, we assume the stresses σ_z and τ_{xz} (at depth $\frac{d}{2}$), are sampled with period b. The sampled stresses are passed through the reconstruction filter resulting in the finger stresses, σ_z and τ_{xz}, at depth d. Using σ_z and σ_x at depth d, ϵ_{zs} is calculated with equation (3). Figure 13 shows sampling of the intermediate stresses used to calculate the normal strain. Figure 14 shows the same information, except that the shear stress is zeroed out after sampling. In both of these simulations, the spatial sampling occurred a quarter period out of phase with respect to the point of the load.

2.5 Grating Input

Given a deflection profile corresponding to a 4.0 mm period grating indenting 2.0 mm, as shown in Figure 15a, we use the procedure in Appendix A to calculate a line load profile that would produce this deflection profile. Knowing that the normal stress is zero where there is no contact with the grating, and limiting our surface normal stress to have only compressive components, we are left with a surface normal stress profile, $\sigma_z(x)$, shown in

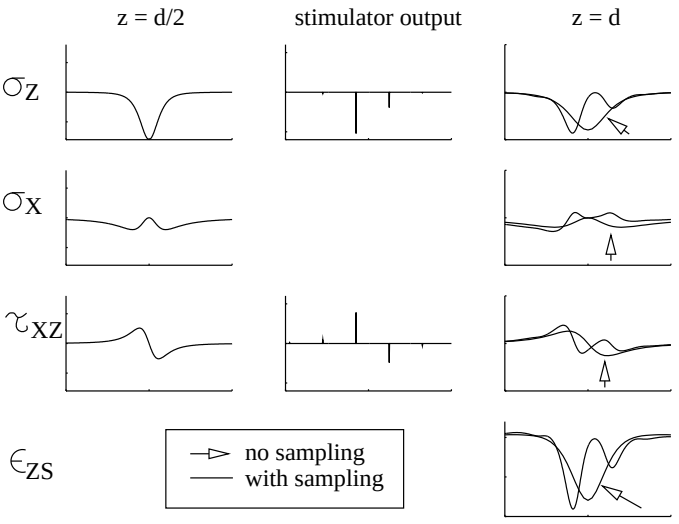

Figure 13: The stresses, σ_z, σ_x, and τ_{xz} and sampled normal strain ϵ_{zs} with ψ = 2.

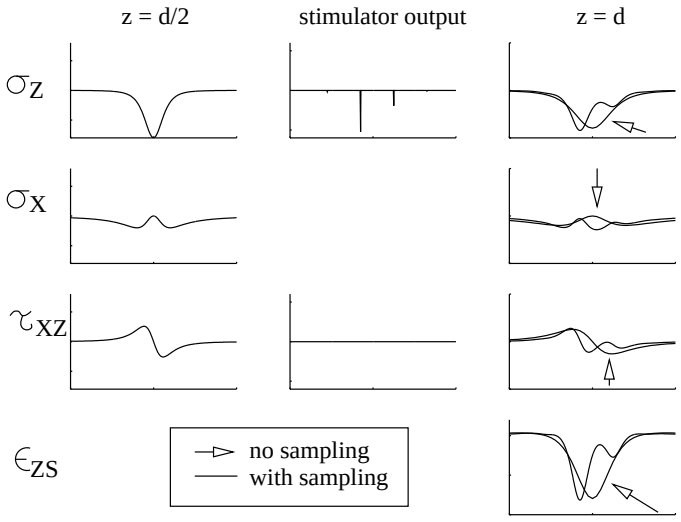

Figure 14: The stresses, σ_z, σ_x, and τ_{xz} and sampled normal strain ϵ_{zs} with ψ = 2 and zeroing of τ_{xz} after sampling.

Figure 15b. The deflection profile corresponding to $\sigma_z(x)$ can be found by convolving $\sigma_z(x)$ and $c(x)$ (Figure 37), and is shown in Figure 15c.

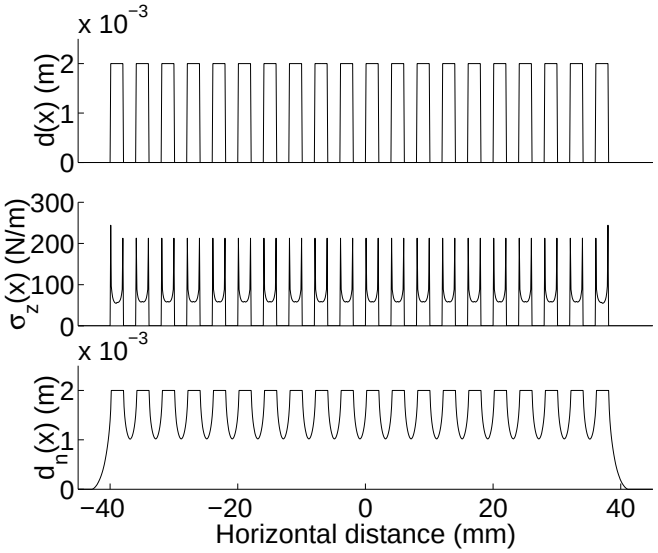

Figure 15: a) Surface (d=0) displacement profile applied, b) Surface normal stress, and c) Displacement profile calculated by convolving normal stress in b) with the c(x) of Figure 37

Modulation Index

For grating profiles and no sampling, a modulation index of the normal strain or normal stress profile can be calculated. The modulation index is a function of grating frequency and thickness of the low-pass elastic layer. The normal subsurface strain or normal stress profile is modeled respectively as:

$$\epsilon_z(x) \sim \alpha_\epsilon(1 + \mu_\epsilon \cos(\omega x)) \quad (12)$$

$$\sigma_z(x) \sim \alpha_\sigma(1 + \mu_\sigma \cos(\omega x)) \quad (13)$$

where α is the scaling factor, μ is the modulation index, and ω is the frequency of the grating. Figure 16 shows the relationship between modulation index of the normal subsurface strain and frequency for the cases with and without shear stress information at depth $d/2$. Figure 17 shows the relationship between modulation index of the normal surface stress applied to the finger and frequency for the same two cases. By using normal surface stress at the interface between the rubber layer and finger, uncertainty whether the mechanoreceptors respond to normal strain, maximum compressive strain, strain energy density, or some other measure does not affect our conclusions.

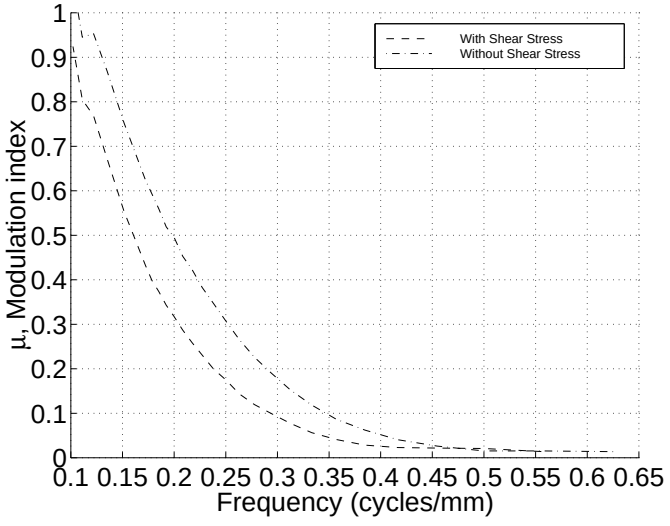

Figure 16: Modulation index of subsurface normal strain vs. frequency. Depth is 2.7 mm (2.0 mm rubber layer + 0.7 mm skin).

2.6 Error Metric for Aliasing

To measure the error in ϵ_z due to aliasing, we define the signal-to-noise ratio to be:

$$SNR = 10log_{10}\left(\frac{\int_{-\infty}^{\infty}\epsilon_z^2(x)dx}{\int_{-\infty}^{\infty}[\epsilon_z(x) - \epsilon_{zs}(x)]^2dx}\right) \quad (14)$$

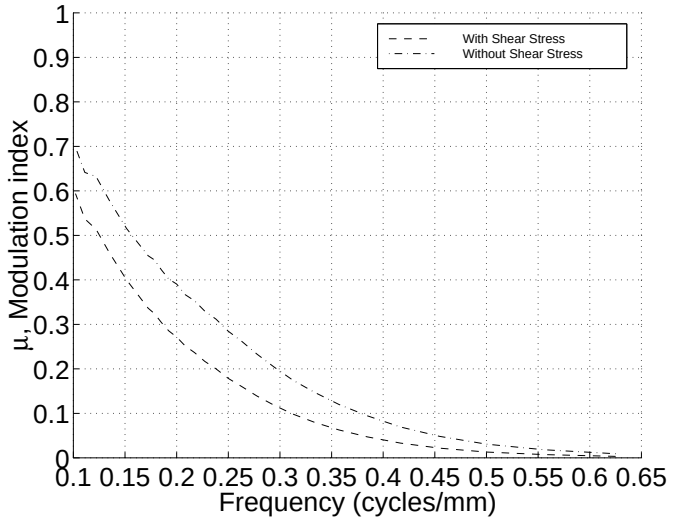

Figure 17: Modulation index of surface normal stress vs. frequency. Depth is 2.0 mm for the rubber layer.

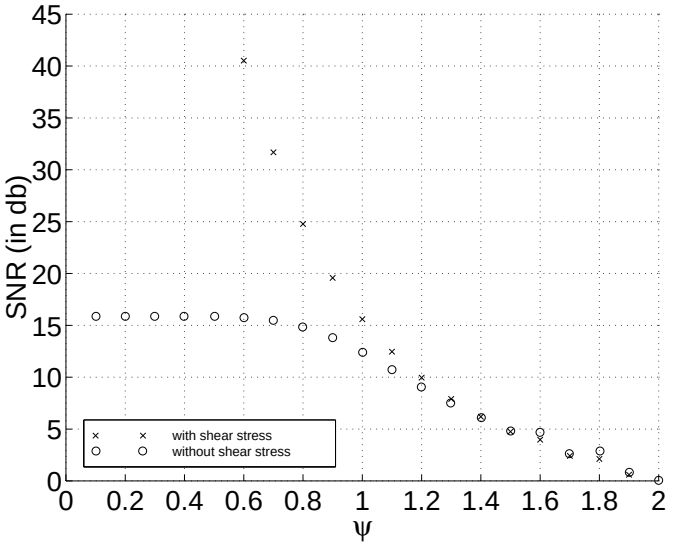

Figure 18: SNR vs. ψ with a normal line load input. If the tactile display can not present shear stress, the SNR is limited to 16 dB

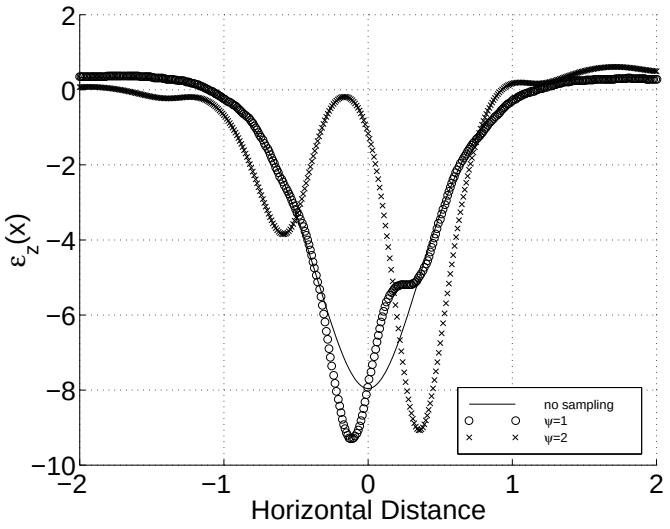

Figure 19: Normal strain in the finger ϵ_z due to a normal line load with no sampling, ψ = 1, and ψ = 2.

Contact type	SNR
line load (normal)	16
line load (30°)	11
block indentor with width 20 (normal)	19
block indentor with width 20 (30°)	7
cylindrical indentor width 20 (normal)	19
cylindrical indentor width 20 (30°)	8

TABLE 1: SNR with no shear stress transmission at z = $\frac{d}{2}$ = 2 and no sampling.

where ϵ_{zs} is the sampled normal strain. In this definition, the signal is the reconstructed normal strain profile without sampling. The noise is the difference between the reconstructed normal strain profile with and without sampling. Figure 18 shows the SNR as a function of ψ, the ratio between array spacing and elastic layer thickness. Figure 19 shows ϵ_z due to a normal line load with no sampling, ψ = 1, and ψ = 2. This model determines how thick the rubber layers should be for a given sampling period and SNR. When sampling, the phase at which the samples are taken is very important. For Figure 19, the worst phase for each ψ was used. Even with no sampling, the SNR of the reconstructed normal strain without transmission of shear stress has an upper bound of 16 dB. Table 1 shows the effects of not transmitting shear stress at depth $\frac{d}{2}$ on the SNR using a variety of inputs and no sampling.

Thus, shear stress information is important for high fidelity tactile stimulators. If a tactile display has $\psi > 1$, then having shear stress information transmitted does not increase the SNR.

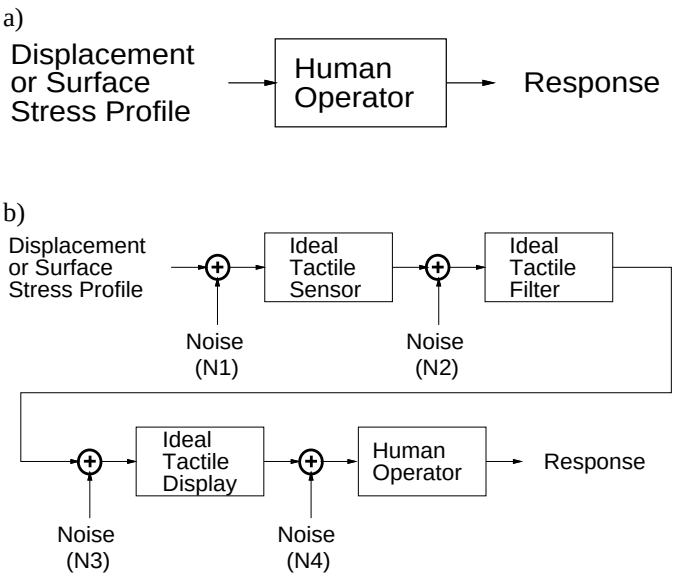

Figure 20: Block diagram representations of a) direct contact and b) contact with a teletaction system and its noise sources

2.7 Noise Models

In this section, we present a model of noise in a teletaction system. Figure 20 shows block diagrams of an ideal frictionless contact through direct touch and a contact made through a teletaction system. Noise source N1 represents friction in the contact and surface imperfections. Noise source N2 represents quantization and aliasing effects of the tactile sensor. Noise source N3 represents the ill-conditioned inverse and interpolation/extrapolation errors from having different sensor and display densities. Noise source N4 represents the quantization and aliasing effects of the tactile display.

With the noise model and the modulation index, we can predict the maximum tolerable noise in the teletaction system. We assume that the human operator is a consistent decision maker. If the stimuli is above threshold, then the response will be positive (i.e. something felt) otherwise it will be negative. Ideally, the response curve will look like a $signum$ function where the threshold is at zero.

We consider only the quantization noise of the tactile display, as precision display design is more difficult than precision sensor design. Starting with the tactile display representation of a smooth pattern (we use a 50% duty cycle square wave), we can determine how large a quantization level the tactile display can have before the human operator feels a non-smooth pattern (Figure 21). The 50% duty cycle square wave represents a tactile display with pin width equal to half the pin spacing. Using the Stress Matching model (Figure 6), we alter the tactile display outputs by δF_{ij} and determine the modulation index of the normal stress at the boundary layer between the rubber layer and human finger. As we can see in Figure 22, variations at lower frequencies are more easily felt. Quantization noise at lower frequencies will have more of an effect than high frequency noise, which might not be felt at all after the lowpass reconstruction filter.

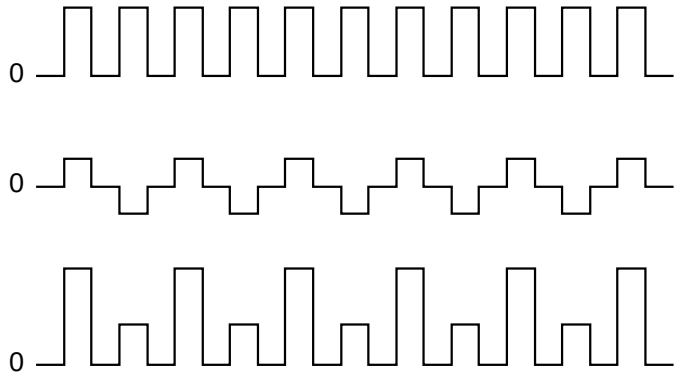

Figure 21: Displacement profile of a) a smooth pattern on the tactile display, b) additive sinusoidal quantization noise, and c) resulting pattern with worst-case quantized force levels.

By determining worst-case bounds on quantization noise source N4, we can back out the maximum tolerable noise at each stage. This oversimplified analysis is a starting point for determining design parameters for each component of the teletaction system.

3 EXPERIMENTS

We conduct four experiments to study various aspects of the human tactile system. Experiment 1 determines the detectable threshold for grating inputs. Experiment 2 tests our theory that reducing shear stress information enhances grating orientation detection. Experiment 3 measures the relaxation parameters for the finger. Experiment 4 measures the effects of viscoelasticity on tactile perception. In experiments 1 and 2, we use rectangular gratings since they are easy to make and approximately represent a sinusoid. In a linear system, the impulse response fully characterizes the system. Unfortunately, the impulse is a mathematical creation, so the frequency response is the best we can do to characterize the system. By testing a range of frequencies, we obtain data which we can correlate to predicted response functions. In experiments 3 and 4, we use a ridge input instead of a grating as the stimulus to concentrate stress.

3.1 Apparatus

For Experiments 1, 3, and 4, we use a Robotworld platform (a planar cartesian manipulator), a four degree of freedom module, a Lord 15/50 force/torque sensor, and two momentary switches. The module has degrees of freedom in X, Y, Z, and Θ (rotation about the Z axis). The force/torque sensor is attached to the modules. Attached to the force/torque sensor are aluminum stimuli mounts as shown in Figure 23a. This system provides accurate real-time position and force control.

In Experiment 1, we use a circular aluminum plate to hold the 12 test patterns, as shown in Figure 23b. The test patterns are wax blocks with 50% duty cycle square wave grating patterns with periods ranging from 3.4 mm to 5.2 mm in 0.2 mm increments and

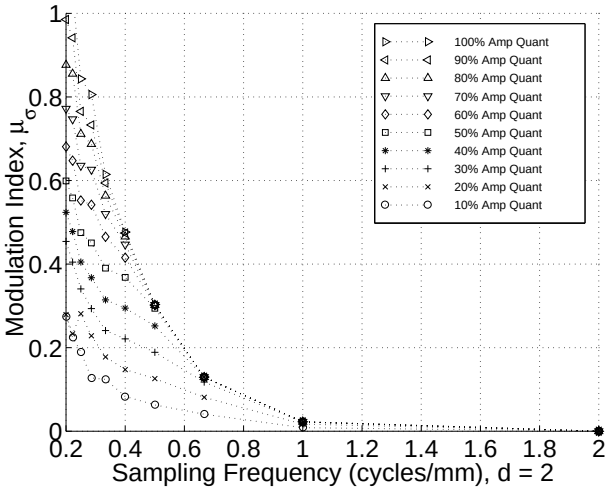

Figure 22: Modulation index of normal stress (with shear stress) vs. sampling frequency for different amplitude quantization levels of a tactile display with a 2 mm reconstruction layer.

two blocks with flat patterns. Subjects wear a 2 mm rubber glove on their index finger. The rubber glove represents the low pass filters necessary on a teletaction system.

In Experiment 2, we use two motorized linear tables and one motorized rotary table, configured in the X,Y, and Θ orientation shown in Figure 24a. This system allows us to quickly present stimuli patterns to the subject in an accurate manner. Two stimuli holders with 10 stimuli are bolted onto the rotary table shown in Figure 24b. Wax blocks with horizontal or vertical grating patterns are placed into the holders. The grating patterns have periods ranging from 2.4 mm to 4.8 mm in 0.6 mm increments with a 50% duty cycle. This range of periods is based on the results of Experiment 1. The rubber layer is either a solid 2 mm piece or two 1 mm pieces with lubricant between them. The lubricant we use to reduce the amount of shear stress is a vegetable oil spray, PAM[1], since other lubricants we tried either dried up too quickly or reacted unfavorably with the silicone rubber.

In Experiments 3 and 4, we use a stair-step plate to hold the 3 test patterns. The three patterns are a smooth block with no pattern, a little ridge (0.1 mm or 0.15 mm), and a large ridge (1.5 mm). The ridges are 5 mm wide and 10 mm long, as shown in Figure 23c. Subjects also wear a 2 mm rubber glove on their index finger in these experiments.

Table 2 summarizes the apparatus we use for the experiments. In all the experiments, the stimuli indents normal to the fingerpad, which eliminates extraneous information from the stimuli sliding across the fingerpad. Rubber layers between the finger and stimuli ensure that no additional surfaces cues, such as small irregularities or thermal information were present. The 2 mm thickness for the rubber layer is based on having an actuator array with 2 mm spacing between the actuators. The 1:1 ratio of spacing and layer thickness gives good anti-aliasing characteristics and an accept-

[1]American Home Products, Inc.

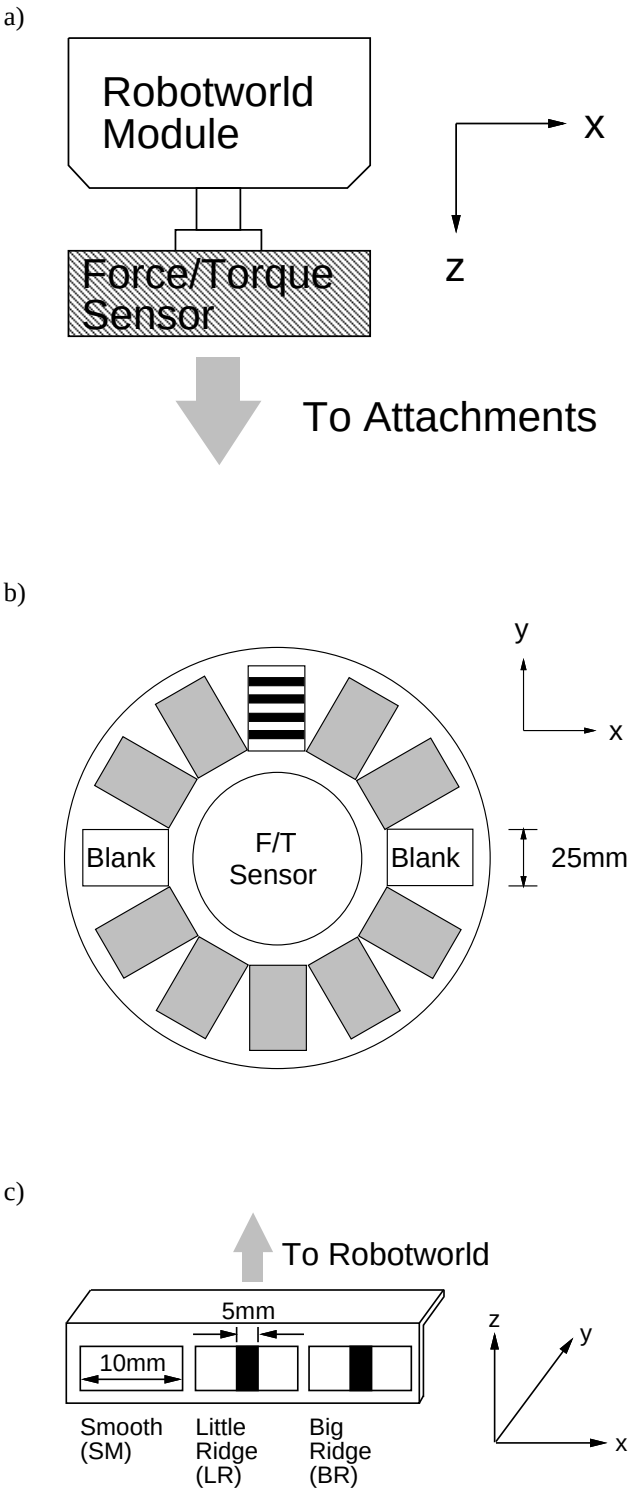

Figure 23: a) Robotworld module and force/torque sensor, b) pattern holder for Experiment 1, and c) pattern holder for Experiments 3 and 4

Exp.	1	2	3	4
Stimuli	Gratings 3.4-5.2 mm period	Gratings 2.4-4.8 mm period	Ridges 0-1.5 mm height	Ridges 0-1.5 mm height
Load	4 N	5-10 N	2.5 N	5.5 N
Duration	2 seconds per pattern	3 seconds per pattern	15+30+15 seconds	3+1.8+2 seconds
Lowpass filter	2 mm glove on finger	2 mm sheet on stimuli with or without lubricant	2 mm glove on finger	2 mm glove on finger
Purpose	Determine minimum detectable grating frequency	Determine effects of shear stress on grating orientation determination	Determine viscoelastic parameters	Determine effects of viscoelasticity on tactile perception

TABLE 2: Summary of apparatus used

able signal to noise ratio (see section 2.6).

3.2 Experiment 1: Grating detection

Our goal is to measure tactile spatial sensitivity through grating detection. In the experiment, the subject extends their index finger and places it on the apparatus (shown in Figure 23b). The finger is kept straight and extended by attaching a wooden splint to the back of the finger. The subjects wear custom molded fingertips made of 2 mm thick rubber, which have contours conforming to the human finger. The finger, rubber fingertip, and splint are immobilized to the test platform by two velcro straps. A series of grating patterns is presented to the subject's finger using the robot module. Using the force sensor, the module controls the plate height to insure that the correct contact force is applied. The pattern is presented for two seconds. The procedure is repeated for another pattern. The pair of patterns is either smooth then grating, or grating then smooth. The subject uses momentary switches to indicate which block has the grating. Each of the ten grated patterns is presented 20 times at a force of 4 N. The experiment takes 12 minutes.

3.3 Experiment 2: Effects of Shear Stress on Grating Orientation Discrimination

Our goal is to measure tactile orientation detection with and without shear stress. In the experiment, the subject extends their right index finger and places it on the finger rest (shown in Figure 24a). The finger rest is adjusted to insure that contact with the stimuli occurs normal to the fingerpad. It is essential that no extraneous information is given to the subject by having the stimuli contact obliquely and slide across the finger when coming to the final contact position. The control program then allows the subject to choose how far the stimuli indents into their finger. The setup is calibrated with a dial indicator to insure that each stimulus indents to the chosen distance with error of less than 25μm. Each of the ten stimuli is presented 15 times in a random order.

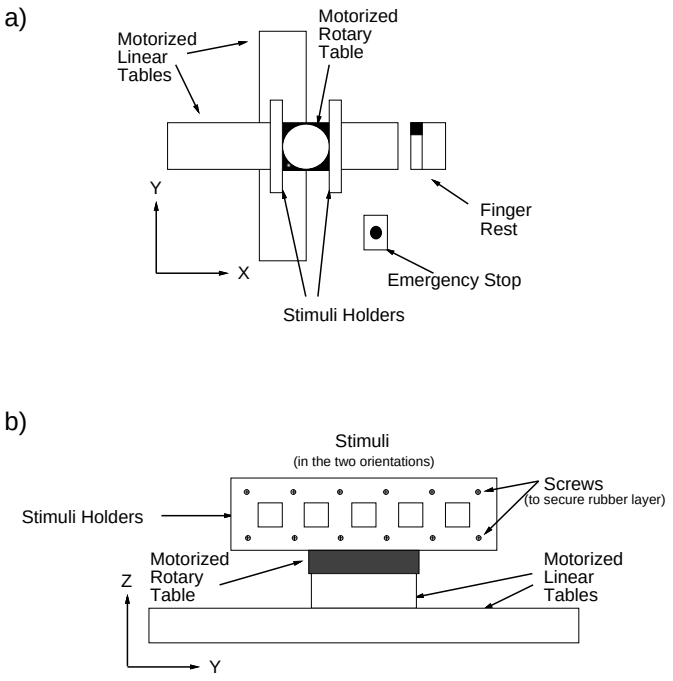

Figure 24: Apparatus for Experiment 2: a) Top view, and b) Front view of the tables, stimuli holder, and stimuli

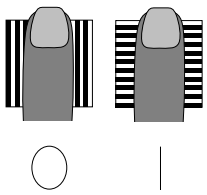

Figure 25: Subjects' response for perceived orientation

Of the ten stimuli, there are 5 distinct frequencies in both orientations. This results in thirty points per frequency tested with half of the points in each orientation.

After the control program presents the stimuli, the subject responds with a "0" or "1" corresponding to which orientation is felt, as shown in Figure 25. The experiment takes approximately 30 minutes. Force measurements show that subjects use 5-10 N of force for the experiment. Forces are constant for each subject, but vary across subjects.

3.4 Experiment 3: Viscoelastic parameters

Our goal is to quantify the viscoelasticity of the human finger. We determine if the finger responds as described by equation 7. We apply a position step to the finger and measure the finger's force response. We then compare the results with the relaxation function shown in Figure 4a. The robot module is commanded to a position that corresponds to a force of 2.5 N exerted on the finger by the block containing a 1.0 mm ridge. After fifteen sec-

Type	First Stimulus	Second Stimulus
1	SM	BR
2	SM	SM
3	BR	SM
4	LR	BR
5	BR	LR

TABLE 3: Trial types and corresponding patterns presented (SM=Smooth, LR=Little Ridge, BR=Big Ridge).

onds, during which the force response of the finger is recorded by the sensor, a position step of 0.5 mm towards the finger is applied by the robot. The force/torque sensor records the force for thirty seconds. Finally, the module is commanded to move back to its original position (i.e. a negative step of 0.5 mm) and the sensor records the force for another fifteen seconds. Due to the limited acceleration and velocity of the robot module, the position step is not instantaneous. It took on the order of 0.6-0.7 seconds to move the 0.5 mm. The above procedure gives a relaxation curve which is used to estimate the parameters of the Kelvin model for each subject.

3.5 Experiment 4: Effects of Viscoelasticity on Tactile Perception

To measure the effects on tactile perception, we determine if the viscoelasticity of the finger pulp has a statistically significant effect on the perception of ridges. The height of the little ridge (LR) is chosen as the threshold where the subject guesses whether they feel a smooth surface or a ridge. The height of the big ridge (BR) is the same one used in the viscoelasticity determination experiment. For this experiment, a force of 5.5N is applied to the finger by the blocks and module.

The experiment consists of 150 trials broken up into five sessions (thirty trials per session). Each trial consists of two blocks being presented to the subject. Each session consists of six of each of the trials outlined in Table 3 in a random order. Note that with three different blocks, each trial could be one of nine (3^2) different types (since two blocks were being presented in each trial). We cut down on the number of trials by only using the combination of blocks that were important in testing whether or not the viscoelasticity of the finger has an effect on touch.

In each trial, the robot module presents the first stimulus with a force of 5.5 N for 3.0 seconds at which point the module moves away from the finger and waits for 1.8 seconds. A waiting period of 1.8 seconds is picked because the average relaxation time constant for the subjects is approximately 2 seconds. Following the wait, the second stimulus is presented at 5.5 N for 2.0 seconds. The subjects push the appropriate momentary switch based on whether or not they felt two ridges in the trial. The conditions for when the subjects are supposed to push each button is outlined in Table 4. The subjects have 10 seconds within which to make a choice.

Choice	Condition(s)
1	Neither input had ridges, Only one input had ridge, Input(s) had negative ridges (grooves)
2	Both inputs had positive ridges

TABLE 4: Choices and condition(s) for each choice

4 DATA AND ANALYSIS

In this section, we will look at the data from each experiment separately. In section 5, we draw conclusions from all the data.

4.1 Experiment 1: Grating detection

The grating detection experiment tests the ability of subjects to discriminate a wax block with a grating pattern versus a wax block with a smooth pattern while wearing a 2 mm thick rubber glove. The experiment was run on 7 voluntary subjects (6 male, 1 female) between 20 and 34 years of age. The index fingers varied in width from 15 mm to 20 mm across the fingerpad. The results of the experiment are shown in Table 5 and Figure 26. Using 75% (the midpoint between random guessing and perfect discrimination) as the threshold level, the threshold grating period for the test subjects varied from 3.6 mm to 5.0 mm. The average of the results are shown in Figure 27 with error bars showing the 95% confidence interval for a proportion with n=20. The average threshold grating period is 4.0 mm.

As predicted from the model, grating detection improves as the period of the grating increases. Looking at the modulation index corresponding to the subjects' threshold grating periods, we can determine how many bits of force resolution is needed for a tactile display. Using normal strain as the criteria for detection, the most sensitive subject could detect a modulation index of 12% while the least sensitive subject could detect a modulation index of 24%. A tactile display with 3 bits of force resolution would be able to present normal strain at 8 different levels, which corresponds to a modulation index of 12.5%.

4.2 Experiment 2: Effects of Shear Stress on Grating Orientation Discrimination

The grating orientation experiment was run on 10 voluntary subjects (9 male, 1 female). The results for the unlubricated case are shown in Table 6 and Figure 28. The results with reduced shear stress information are shown in Table 7 and Figure 29. The ability to discriminate grating orientation increased at all frequencies when there is reduced shear stress information.

The averages of the data are shown in Figure 30. To quantify the significance, we applied the χ^2 test with 1 degree of freedom [Walpole and Myers 1993]. We use the average as the expected frequency.

The calculated χ^2 values are as follows:

Period (mm)	2.4	3.0	3.6	4.2	4.8
χ^2	2.41	4.98	7.29	34.3	28.7

The results of the shear and reduced shear experiments are from

Period (mm)	3.4	3.6	3.8	4.0	4.2
Subject 1:	11	13	11	12	16
Subject 2:	8	11	10	13	15
Subject 3:	9	14	13	17	15
Subject 4:	9	15	16	18	18
Subject 5:	13	12	15	17	18
Subject 6:	7	17	14	11	13
Subject 7:	11	15	16	16	19
Mean	9.71	13.9	13.6	14.9	16.3

Period (mm)	4.4	4.6	4.8	5.0	5.2
Subject 1:	16	18	18	17	19
Subject 2:	12	14	14	18	20
Subject 3:	20	19	20	20	20
Subject 4:	16	19	20	20	19
Subject 5:	18	18	18	19	20
Subject 6:	17	16	18	16	19
Subject 7:	18	19	17	20	19
Mean	16.7	17.6	17.9	18.6	19.4

TABLE 5: Raw data from grating detection experiments. Data are number correct out of 20 trials per period per subject.

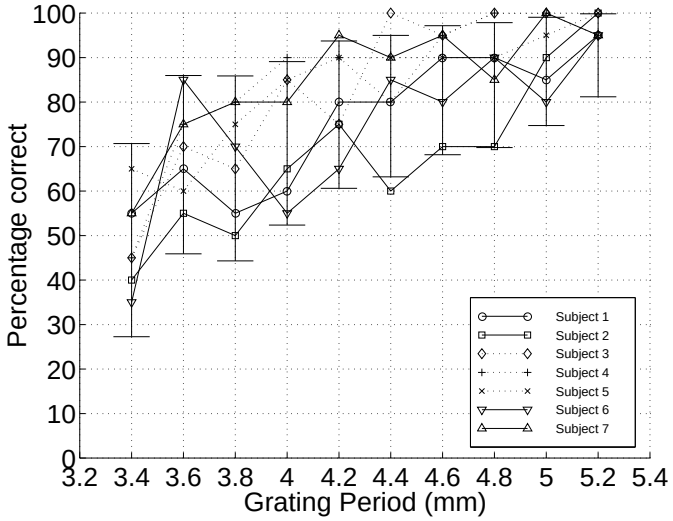

Figure 26: Graph of the data from grating detection experiment with error bars representing the 95% confidence intervals for a proportion. Each point represents the results of 20 trials.

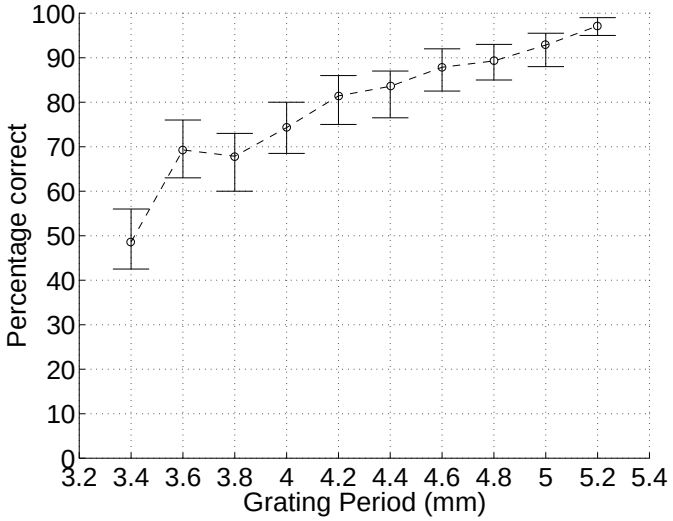

Figure 27: Average of the data for grating detection experiment with error bars representing the 95% confidence intervals for a proportion. Each point represents the results of 140 trials.

	Shear				
Period (mm)	2.4	3.0	3.6	4.2	4.8
Subject 1:	12	15	23	28	29
Subject 2:	20	16	16	22	26
Subject 3:	13	14	11	21	22
Subject 4:	17	15	17	23	12
Subject 5:	17	15	18	27	23
Subject 6:	13	22	18	25	26
Subject 7:	13	15	15	18	21
Subject 8:	12	18	15	25	27
Subject 9:	15	15	20	23	28
Subject 10:	7	15	19	18	20
Mean	13.9	16.0	17.2	23.0	23.4

TABLE 6: Raw data from grating orientation experiments. Data are number correct out of 30 trials per period per subject.

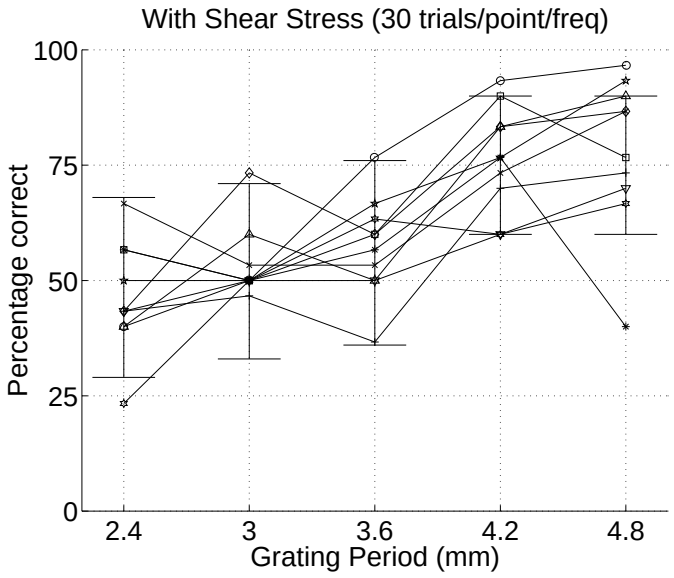

Figure 28: Graphs of the data from grating orientation experiment with error bars representing the 95% confidence intervals for a proportion. Each point represents the results of 30 trials.

Reduced Shear					
Period (mm)	2.4	3.0	3.6	4.2	4.8
Subject 1:	12	21	24	26	30
Subject 2:	21	15	15	30	29
Subject 3:	20	17	15	30	28
Subject 4:	17	27	27	27	30
Subject 5:	16	18	18	29	30
Subject 6:	14	28	21	28	25
Subject 7:	15	15	15	26	26
Subject 8:	14	14	24	30	29
Subject 9:	16	18	23	29	28
Subject 10:	13	14	22	26	25
Mean	15.8	18.7	20.4	28.1	28.0

TABLE 7: Raw data from grating orientation experiments. Data are number correct out of 30 trials per period per subject.

different populations for grating periods greater than or equal to 3.0 mm (95% probability, $\chi^2 > 3.84$). Since 2.4 mm was below the detectable threshold with a 2.0 mm thick anti-aliasing layer, it is not surprising that there was no significant difference between the shear and reduced shear data.

4.3 Experiment 3: Viscoelastic parameters

The experiment was run on six test subjects (3 male, 3 female) between 21 and 35 years of age. In section 2.2, we presented a mechanical model of the finger consisting of springs and dashpots. After running the experiment, a relaxation function was obtained for each of the six subjects. Figure 31 shows a relaxation function (to a position step) for a rubber layer. There is a very small viscoelastic effect. Figure 32 shows a relaxation function for subject 2. The viscoelastic effect is very apparent up to approximately 15 seconds (just before the 0.5 mm position step). The other subjects exhibited similar relaxation functions.

The relaxation function for the Kelvin model (equation (7)) can be rewritten more generally as

$$k(t) = A + Be^{-tc} \tag{15}$$

where

$$A = E_R,\ B = \frac{-E_R(\tau_\epsilon - \tau_\sigma)}{\tau_\epsilon},\ c = \frac{1}{\tau_\epsilon} \tag{16}$$

We used a nonlinear curve fitting algorithm based on the simplex algorithm to fit an exponential function of the form given in equation (15) to the force response taken in the first 15 seconds for each subject. Figure 33 shows an example of the curve fitting for the relaxation curve of the subject shown in Figure 32. The data

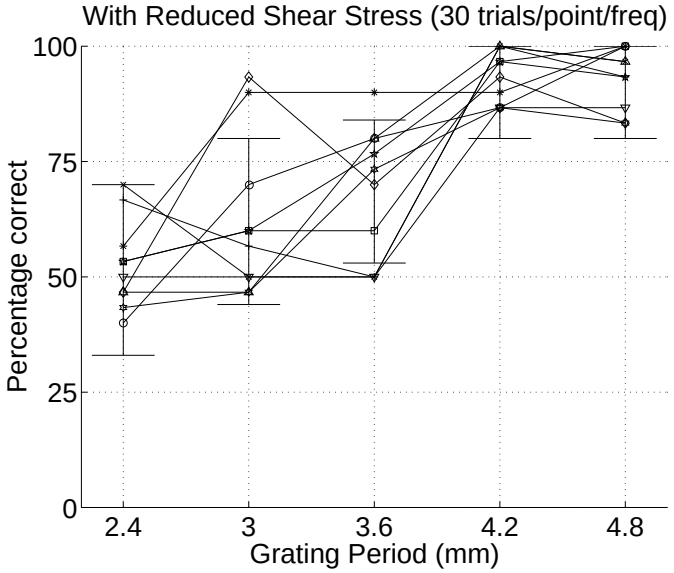

Figure 29: Graphs of the data with error bars representing the 95% confidence intervals for a proportion. Each point represents the results of 30 trials.

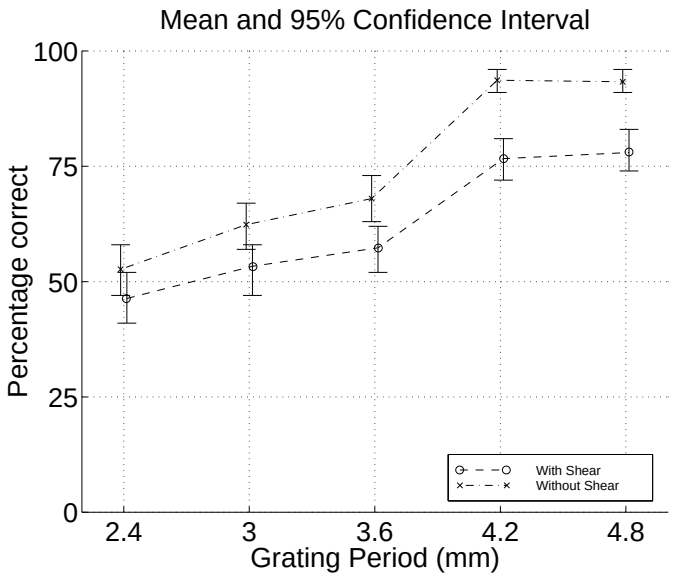

Figure 30: Averages of the data from 10 subjects. Each point represents the average results of 300 trials.

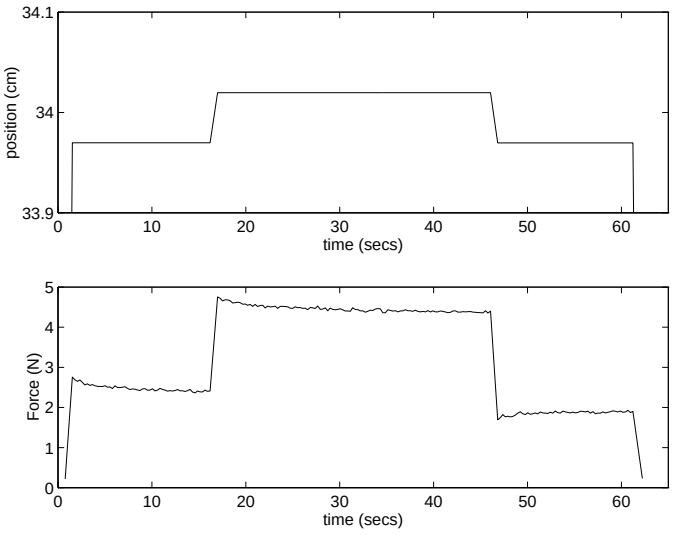

Figure 31: Relaxation function for a rubber layer.

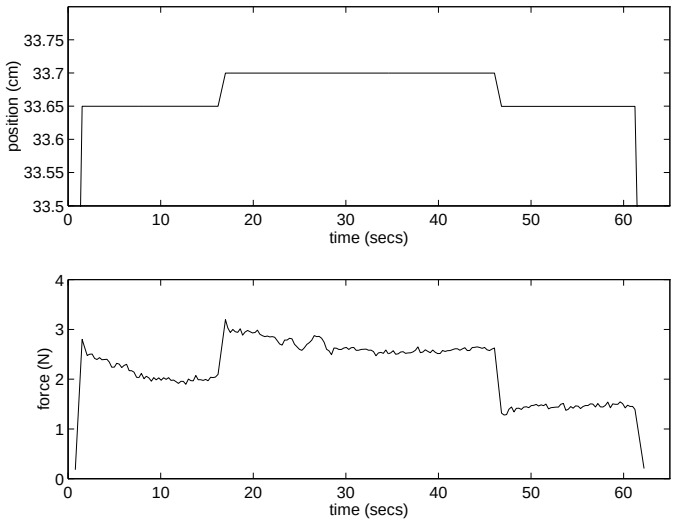

Figure 32: Relaxation function for subject 2.

Subject	A	B	c	τ_ϵ	τ_σ
1	2.29	1.15	0.70	1.42	2.14
2	1.95	1.10	0.26	3.90	6.11
3	2.20	0.89	0.58	2.71	3.82
4	2.24	0.67	0.35	2.81	3.65
5	2.04	0.85	0.30	3.38	4.78
6	2.59	0.34	0.26	3.88	4.39

TABLE 8: Parameter values of the viscoelastic model of the finger

for the other subjects is shown in Table 8. The value τ_σ can be found by substituting the known values into the equation for B in equation (16).

According to equation (8) and Figure 4b, after the constant force input is removed, the finger pulp (due to viscoelastic creep) exponentially deforms back to its original location with time-constant equal to τ_σ. We will ignore all other constants for this analysis. When a ridge is pressed against the finger with a force of 5.5 N for 3 seconds, the deformation of the fingerpulp is normalized to one. Zero corresponds to the finger pulp in its original location. Waiting 1.8 seconds after the pattern is removed, the finger is at some position depending on the value of τ_σ for each subject. Table 9 shows the deformation in normalized units for each subject. The first subject's finger retains 43% of the input while the second subject's finger retains 74% of the input.

4.4 Experiment 4: Effects of Viscoelasticity on Tactile Perception

This experiment was run on the same six subjects tested in Experiment 3. The responses of the experiment were either $choice1$ or $choice2$ as described in Table 4. The performance, as indicated by fraction of trials that a subject picked $choice2$ for each type of trial, is shown in Figure 34. The most consistent effect observed

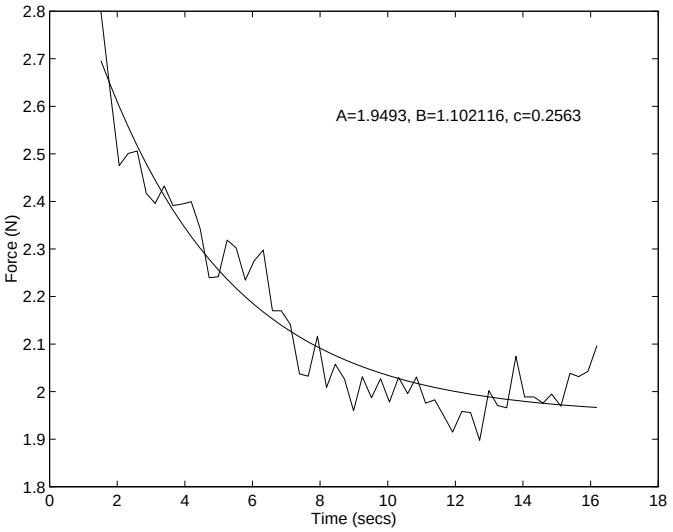

Figure 33: Exponential fit for relaxation function.

Subject	Position of finger
1	0.43
2	0.74
3	0.62
4	0.61
5	0.69
6	0.66

TABLE 9: Position of finger 1.8 seconds after a BR pattern is removed from the fingerpad (in normalized units where zero corresponds to finger in starting location, and one corresponds to location of finger after a BR pattern has been applied for 3 seconds

is the greater detection of two ridges in (LR,BR) than (BR,LR) as shown in Figure 35. Refer to Table 3 to see what input patterns were presented for each type.

We apply a χ^2 test to quantify the statistical significance of the difference in proportions between trials of types 1 and 3 and types 4 and 5 for each subject. The frequencies and χ^2-values for each subject are shown in Table 10. For a level of significance of 0.05 (i.e. 95% confidence level), with 1 degree of freedom, $\chi^2 > 3.84$. From the table we can see that subjects 4 and 6 were well within the 95% confidence level of the means not being equal for trials of types 1 and 3. We can also safely conclude that the the means for trials of types 4 and 5 were not equal for subjects $2, 3, 5$, and 6. Subject 4 fell within the 0.10 level of significance for types 4 and 5. Subject 1 did not show any significant difference in detecting ridges.

5 CONCLUSIONS AND FUTURE WORK

The core results from the experiments are tabulated in Table 11. This series of experiments provides some of the necessary param-

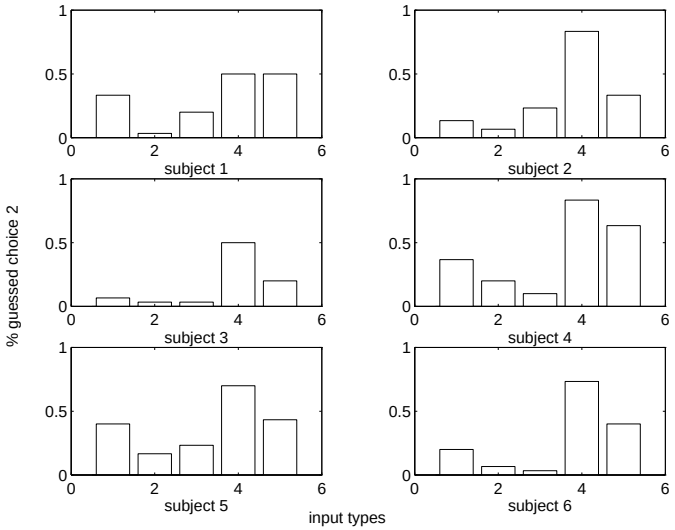

Figure 34: Fraction of trials of all types (1=(SM,BR), 2=(SM,SM), 3=(BR,SM), 4=(LR,BR), 5=(BR,LR)) where the subject 'felt two ridges' (choice 2).

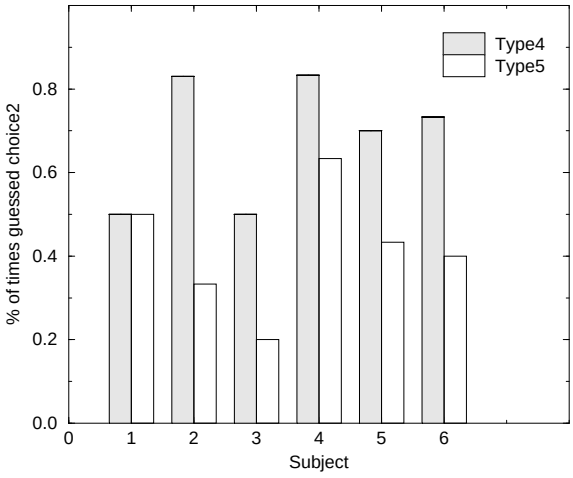

Figure 35: Fraction of trials of types 4 (LR,BR) and 5 (BR,LR) for which 'felt two ridges' (choice 2) was picked as a response.

#	Type 1 SM-BR	Type 3 BR-SM	χ^2	Type 4 LR-BR	Type 5 BR-LR	χ^2
1	0.33	0.20	1.36	0.50	0.50	0.0
2	0.13	0.23	1.00	0.83	0.33	15.43
3	0.07	0.03	0.35	0.50	0.20	5.93
4	0.37	0.10	5.96	0.83	0.63	3.07
5	0.40	0.23	1.93	0.70	0.43	4.35
6	0.20	0.03	4.05	0.73	0.40	6.77

TABLE 10: Proportion for feeling two ridges in contact for types 1,3 and t ypes 4,5 and χ^2 values for each subject. (N=30)

Exp.	Results
1	Grating detection increases with period. On average, a 1-bit tactile display gives 75% correct with 4.0 mm grating period. A 3-bit tactile display is needed for a 10.0 mm grating period.
2	Grating orientation discrimination is significantly enhanced by reducing the shear stress between the rubber layers. On average, 75% correct at 3.8 mm grating period for reduced shear stress and 4.2 mm for full shear stress cases. The signal to noise ratio is higher for the reduced shear stress case. Again, a 3-bit tactile display is needed for a 10.0 mm grating period to be indistinguishable from a smooth pattern given a 1-bit sinusoidal error.
3	Determined the stress-relaxation and creep parameters for six subjects. The human fingerpad retains 43% to 74% (average of 62.5%) of the indentation 1.8 seconds after the indentation is released.
4	Detection of ridges correlates well with the percent residual deformation of the fingerpad.

TABLE 11: Compiled results from the four experiments using a 2 mm layer.

eters for designing a teletaction system. From experiment 1, objects with spatial frequencies < 0.25 cycles/mm are readily perceived through a 2 mm rubber layer. Thus, a tactile display should have 0.5 samples/mm by the Nyquist criterion, and array spacing to rubber layer ratio $\psi < 2$. From experiment 2, designing a tactile display to match only the normal stress is sufficient when the tactile sensor probes objects normal to the sensor surface in a slippery environment. The slippery environment enhances the high frequency content of the object detected by the tactile sensor.

Since the square grating is effectively equivalent to a very densely packed 1-bit displacement tactile display for our experiments, we can determine the necessary number of bits needed based on fidelity and lowest frequency to be presented. At a 4.0 mm grating period, which corresponds to a normal stress modulation index of 0.18, subjects correctly identified the grating pattern 75% of the time, or alternatively, 25% of the time, the grating pattern was undetectable. By using Figure 17, a 1-bit tactile display presenting a 10.0 mm period grating correlates

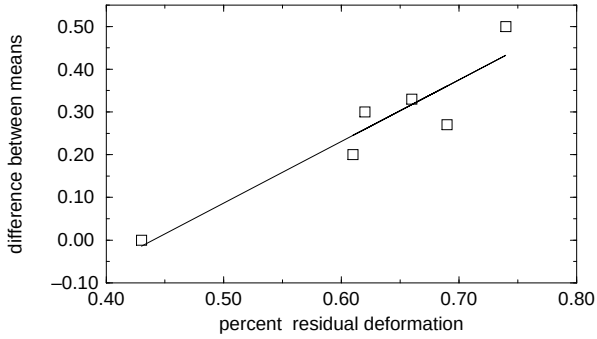

Figure 36: Correlation between the difference of means for type 4 and 5 stimuli with percent residual deformation of the fingerpad 1.8 seconds after a ridge stimuli has been removed. (correlation coefficient $\rho = 0.92$)

to a normal stress modulation index of 0.60. In order to reduce the normal stress modulation index to the 25% undetectable level (modulation index of 0.18), we need a 3-bit displacement tactile display. With 3 bits, a quantized sinusoidal 1-bit error will only generate a 0.60 * $(0.5)^{(3-1)}$ = 0.15 modulation index, which is less than the required 0.18 for the 25% undetectable level. For higher fidelity, we look at when the pattern was 60% detectable, or 40% of the time, the grating pattern was undetectable, which corresponds to a 3.5 mm grating period (frequency = 0.29 cycles/mm). This level corresponds to a 0.13 normal stress modulation index (see Figure 17). At a 10.0 mm grating period, we need $\approx$ 3.5 bits of displacement resolution.

Experiments 3 and 4 show the viscoelastic effects of the human finger and the effects on tactile perception. Figure 36 shows the strong correlation between slow skin relaxation and perceptual interference. Afterimages in the skin must be taken into account when designing the control algorithm for the teletaction system. The large afterimage reduces the required display amplitude and temporal resolution for high stress inputs.

More studies need to be performed to correlate the pattern presented by a teletaction system and the pattern felt by direct touch. With a better understanding of the spatial, temporal, and sensitivity of the human tactile system, we will be able to design a better teletaction system. As actuator technology advances, we will be able to fabricate small tactile displays for use on master controller devices, such as laparoscopic instruments and joysticks.

6 ACKNOWLEDGEMENTS

We thank K. Chiang, J. Yan, D. Pick, and C. Wagner for useful comments and discussions. The financial support by NSF grant IRI-9531837 is gratefully acknowledged.

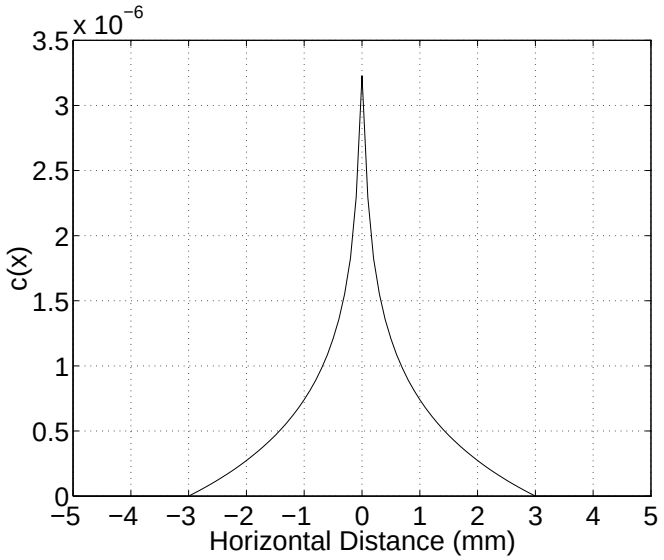

Figure 37: Deflection profile, c(x), caused by a line load at x=0 with x_0 = 25 μ m and x_b = 3.0 mm

APPENDIX: CONVERSION FROM DISPLACEMENT TO STRESS

The fundamental relation between a surface deflection and a normally applied line load is shown in Figure 37, and given by:

$$c(x) = \begin{cases} \frac{2}{\pi E} log \frac{x_b}{x_o}, & |x| < x_o \\ \frac{2}{\pi E} log \frac{x_b}{x}, & x_o < |x| < x_b \\ 0, & x_b < |x| \end{cases} \quad (17)$$

where x_0 is half the width of the applied line load, and x_b is the distant boundary. So from equation 17, the line load has a constant deflection in the width of application, decays logarithmically until the distant boundary, and is zero outside of the distant boundary. We used the same values as [Phillips and Johnson 1981], x_0 = 25 μm and x_b = 3 mm.

As in [Phillips and Johnson 1981], we assume that the deflection is proportional to the magnitude of the line load, the deflection function $c(x)$ is space invariant, and the overall deflection profile is the superposition of deflection profiles from the individual line loads. Discretizing $c(x)$, we can represent the discretized deflection profile d(x_i) as:

$$d(x_i) = \sum_{j=1}^{n} c(x_i - x_j) p(x_j) \quad (18)$$

where $p(x_j)$ is the discretized line load profile, and n is the number of points representing the profiles. Rewriting equation 18 as a matrix operation, we express the best line load profile as a least squares problem. Given a deflection profile d and the deflection matrix C (calculated from $c(x)$), we can find p as follows:

$$Cp = d \quad (19)$$

$$p = (C^T C)^{-1} C^T d \quad (20)$$

In our case, p and d are the same length, so

$$p = C^{-1} d \quad (21)$$

REFERENCES

[1] Bliss, J. C., "A Relatively High-Resolution Reading Aid for the Blind", *IEEE Trans. on Man-Machine Sys.*, vol. 10, pp. 1-9, 1969.

[2] Caldwell, D. G., Tsagarakis, N., and Giesler, C., "An Integrated Tactile/Shear Feedback Array for Stimulation of Finger Mechanoreceptor", *IEEE Int. Conf. Rob. and Auto.*, vol. 1, pp. 287-292, Detroit, MI, May 1999.

[3] Cohn, M. B., Lam, M., and Fearing, R.S., "Tactile Feedback for Teleoperation", *SPIE Telemanip. Tech.*, vol. 1833, pp. 240-254, Boston, MA, November 15-16, 1992.

[4] Domenici, C. and DeRossi, D., "A Stress-component-selective tactile sensor array", *Sensors and Actuators A*, vol. 13, pp. 97-100, 1992.

[5] Ellis, R. E. and Qin, M., "Singular Value and Finite-Element Analysis of Tactile Shape Recognition", *IEEE Int. Conf. on Robotics and Automation*, vol. 3, pp. 2529-2535, San Diego, CA, May 8-13, 1994.

[6] Fearing, R. S., "Tactile Sensing Mechanisms", *Int. Jnl. of Robotics Research*, vol. 9, no. 3, pp. 3-23, June 1990.

[7] Fischer, H., Neisius, B., and Trapp, R., "Tactile Feedback for Endoscopic Surgery" in *Interactive Technology and New Paradigm for Healthcare*, edited by K. Morgan, R. M. Satava, H. B. Sieburg, R. Mattheus, J. P. Christensen, pp. 114-117, IOS Press 1995.

[8] Fung, Y. C., "Biomechanics: Mechanical Properties of Living Tissues", Springer-Verlag, 1993.

[9] Ghodssi, R., Beebe, D. J., White, V., and Denton, D. D., "Development of a Tangential Tactor Using a LIGA/MEMS Linear Microactuator Technology", *1996 Int. Mech. Eng. Cong. and Exposition, Microelectromechanical Systems*, DSC Vol. 59, pp. 379-386, Nov. 17-22, 1996.

[10] Gray, B. L. and Fearing, R. S., "A surface-micromachined microtactile sensor array", *IEEE Int. Conf. Rob. and Auto.*, vol. 1, pp. 1-6, Minneapolis, MN, April 1996.

[11] Hagner, D. G. and Webster, J. G., "Telepresence for Touch and Proprioception in Teleoperator Systems", *IEEE Trans. on Systems, Man, and Cybernetics*, vol. 18, no. 6, pp. 1020-1023, November/December 1988.

[12] Hasser C. J. and Daniels, M. W., "Tactile Feedback with Adaptive Controller for a Force-Reflecting Haptic Display", *15th Southern Biomedical Engineering Conf.*, pp. 526-533, Dayton, OH, March 29-31, 1996.

[13] Howe, R.D., "Tactile sensing and control of robotic manipulation", *Advanced Robotics*, vol. 8, no. 3, pp. 245-61, 1994.

[14] Howe, R. D., Peine, W. J., Kontarinis, D. A., and Son, J. S., "Remote Palpation Technology", *IEEE Eng. in Med. and Bio. Mag.*, pp. 318-323, May/June 1995.

[15] Johansson, R. S., Landström, U., and Lundström, R., "Responses of Mechanoreceptive Afferent Units in the Glabrous Skin of the Human Hand to Sinusoidal Displacements", *Brain Research*, vol. 244, p. 17-25, 1982.

[16] Johnson, K. L., Contact Mechanics, Cambridge University Press, 1985.

[17] Johnson, K. O. and Phillips, J. R., "Tactile Spatial Resolution I. Two Point Discrimination, Gap Detection, Grating Resolution, and Letter Recognition", *J. Neurophysiology*, vol. 46, no. 6, pp. 1177-1191, 1981.

[18] Kaczmarek, K. A., Webster, J. G., Bach-y-Rita, P., and Tompkins, W. J., "Electrotactile and Vibrotactile Displays for Sensory Substitution Systems", *IEEE Trans. on Biomedical Engineering*, vol. 38, no.1, pp. 1-16, Jan. 1991.

[19] Lamotte, R. H. and Srinivasan, M. A., "Tactile Discrimination of Shape: Responses of Slowly Adapting Mechanoreceptive afferents to a step stroked across the monkey fingerpad", *J. Neuroscience*, vol. 7, no. 6, pp. 1655-1671, June 1987.

[20] Lederman, S. J., "Heightening Tactile Impressions of Surface Texture", *Active Touch*, ed. G. Gordon. Oxford: Pergamon Press, pp. 205-214, 1978.

[21] Loomis J. M. and Lederman S. J., "Tactual Perception", in *Handbook of Perception and Human Performance* , edited by K.R. Boff, L. Kaufman and J.P. Thomas, pp. 31-1:31-41, John Wiley and Sons: New York, 1986.

[22] Maeno, T. and Kobayashi, K., "FE Analysis of the Dynamic Characteristics of the Human Finger Pad in Contact with Objects with/without Surface Roughness", *IMECE Proc. of the ASME Dyn. Sys. and Control Div.*, vol. 64, pp. 279-286, Anaheim, CA, November 1998.

[23] Nicolson, E. J. and Fearing, R. S., "Sensing Capabilities of Linear Elastic Cylindrical Fingers", *IEEE/RSJ Int. Conf. on Intelligent Robots and Systems*, vol. 1, pp. 178-85, Yokohama, Japan, July 1993.

[24] Nicolson, E. J. and Fearing, R. S., "The Reliability of Curvature Estimates from Linear Elastic Tactile Sensors", *IEEE Int. Conf. on Robotics and Automation*, vol. 1, pp. 1126-33, Nagoya, Japan, May 1995.

[25] Pawluk, D. T. V. and Howe, R. D., "Dynamic Lumped Element Response of the Human Fingerpad", *ASME J. of Biomechanical Engineering*, vol. 121, no. 2, pp. 178-83, April 1999.

[26] Pawluk, D. T. V., van Buskirk, C. P., Killebrew, J. H., Hsiao, S. S., and Johnson, K. O., "Control and Pattern Specification for a High Density Tactile Array", *IMECE Proc. of the ASME Dyn. Sys. and Control Div.*, vol. 64, pp. 97-102, Anaheim, CA, November 1998.

[27] Phillips, J. R. and Johnson, K. O., "Tactile Spatial Resolution II. Neural representation of bars, edges, and gratings in monkey primary afferents", *J. Neurophysiology*, vol. 46, no. 6, pp. 1192-1203, 1981.

[28] Phillips, J. R. and Johnson, K. O.,"Tactile Spatial Resolution III. "A Continuum Mechanics Model of Skin Predicting Mechanoreceptor Responses to Bars, Edges, and Gratings", *J. Neurophysiology*, vol. 46, no. 6, pp. 1204-1225, 1981.

[29] Shimoga, K. B., "Finger Force and Touch Feedback Issues in Dextrous Telemanipulation", *NASA-CIRSSE Int. Conf. on Intelligent Robotic Systems for Space Exploration*, Troy, NY, September 30 - October 1, 1992.

[30] Shimojo, M., "Spatial Filtering Characteristic of Elastic Cover for Tactile Sensor", *IEEE Int. Conf. on Robotics and Automation*, pp. 287-292, San Diego, CA, May 8-13, 1994.

[31] Sladek, E. M. and Fearing, R. S., "The Dynamic Response of a Tactile Sensor", *IEEE Int. Conf. on Robotics and Automation*, Cincinnati, OH, May 1990.

[32] Srinivasan, M. A. and Dandekar, K., "An Investigation of the Mechanics of Tactile Sense Using Two Dimensional Models of the Primate Fingertip", *J. Biomechanical Engineering*, vol. 118, pp. 48-55, 1996.

[33] Valbo, A. B. and Johanson, R. S. "Detection of Tactile Stimuli. Thresholds of Afferent Units related to psychophysical thresholds in the human hand", *J. Physiology*, vol. 297, pp. 405-422, 1979.

[34] Walpole R. and Myers R., "Probability and Statistics for Engineers and Scientists", Macmillan Publishing Company, 1993.

[35] Weisenberger, J. M., Krier, M. J., Rinker, M. A., "Resolution of Virtual Grating Orientation with 2-DOF and 3-DOF Force Feedback Systems", *IMECE Proc. of the ASME Dyn. Sys. and Control Div.*, vol. 64, pp. 295-301, Anaheim, CA, November 1998.